

# Interplay between localized and itinerant $d$ electrons in a frustrated metallic antiferromagnet, $2H\text{-AgNiO}_2$

A. I. Coldea<sup>1</sup>, A. Carrington<sup>1</sup>, R. Coldea<sup>1</sup>, L. Malone<sup>1</sup>, A.F. Bangura<sup>1</sup>, M. D. Johannes<sup>2</sup>, I. I. Mazin<sup>2</sup>, E.A. Yelland<sup>1</sup>, J. G. Analytis<sup>1</sup>, J.A.A.J. Perenboom<sup>4</sup>, C. Jaudet<sup>5</sup>, D. Vignolles<sup>5</sup>, T. Sorgel<sup>3</sup>, M. Jansen<sup>3</sup>

<sup>1</sup>*H. H. Wills Physics Laboratory, Bristol University, Tyndall Avenue, BS8 1TL, United Kingdom*

<sup>2</sup>*Code 6393, Naval Research Laboratory, Washington, D.C. 20375, USA*

<sup>3</sup>*Max-Planck-Institut für Festkörperforschung, Heisenbergstr. 1, 70569 Stuttgart, Germany*

<sup>4</sup>*High Field Magnet Laboratory, IMM, Radboud University, 6525 ED Nijmegen, The Netherlands and*

<sup>5</sup>*Laboratoire National des Champs Magnétiques Pulsés, 31400 Toulouse, France*

(Dated: September 24, 2018)

We report the electronic and magnetic behaviour of the frustrated triangular metallic antiferromagnet  $2H\text{-AgNiO}_2$  in high magnetic fields (54 T) using thermodynamic and transport measurements. Here localized  $d$  electrons are arranged on an antiferromagnetic triangular lattice nested inside a honeycomb lattice with itinerant  $d$  electrons. When the magnetic field is along the easy axis we observe a cascade of field-induced transitions, attributed to the competition between easy-axis anisotropy, geometrical frustration and coupling of the localized and itinerant system. The quantum oscillations data suggest that the Fermi surface is reconstructed by the magnetic order but in high fields magnetic breakdown orbits are possible. The itinerant electrons are extremely sensitive to scattering by spin fluctuations and a significant mass enhancement ( $\sim 3$ ) is found.

PACS numbers: 71.18.+y, 71.27.+a, 72.80.Le, 74.70.-b, 78.70.Gq

Strongly-interacting electrons in triangular layers display a variety of correlated phases stabilized by the frustrated lattice geometry; for example, spin liquid in a triangular organic Mott insulator in the close proximity of pressure-driven superconducting state [1] or superconductivity in water-intercalated  $\text{Na}_x\text{CoO}_2$  [2]. High magnetic fields can be used as a tuning parameter to manipulate the electronic ground state and drive transitions to novel phases and here we explore such physics in the metallic triangular antiferromagnet,  $2H\text{-AgNiO}_2$ , proposed to realize a novel paradigm for charge order in orbitally-degenerate weakly-itinerant systems [3, 4]. Interestingly, below the charge order transition at 365 K the system remains metallic, and a rather unusual electronic ground state is proposed by band-structure calculations: a triangular lattice of electron-rich and localized Ni1 sites ( $\text{Ni}^{2+}$ ,  $S = 1$ ) nested inside a honeycomb lattice of  $\text{Ni}^{3.5+}$  where electrons remain itinerant (see Fig.1f). A novel magnetic ground state is observed at low temperatures where the spins of the localized Ni1 sites order in a collinear structure of alternating stripes, whereas the itinerant electrons remain magnetically unordered [4]. In  $\text{AgNiO}_2$  the spin anisotropy and magnetic interactions are sufficiently low that a large part of the whole magnetic phase diagram in field is experimentally accessible and here we reveal a cascade of field-induced phases, with itinerant electrons being strongly affected by the spin fluctuations near the phase boundaries, with reconstructions of the Fermi surface and magnetic breakdown orbits becoming possible at high field.

Torque measurements are well suited for investigating both changes in the magnetic ground state, manifested in kink anomalies in the torque response, as well as the Fermi surface (FS) of the itinerant electrons, via observation of quantum oscillations in the magnetization (de Haas-van Alphen effect). Torque,  $\tau = \mathbf{m} \times \mathbf{B}$ , in magnetic materials is caused by

anisotropy, and measures the misalignment of the magnetization,  $\mathbf{m}$ , with respect to the applied magnetic field  $\mathbf{B}$ . We measured the overall torque response using a sensitive piezoresistive cantilever technique. Specific heat was measured using a purpose built calorimeter which uses both a long relaxation and an *ac* relaxation method. Hexagonal-like single crystals (typical size  $\sim 120 \times 100 \times 10 \mu\text{m}^3$ , 6 crystals were investigated) were grown using a solid-state route under high oxygen pressures [5]). The residual interlayer resistivity ratio was  $\sim 250$ . Measurements were performed at low temperatures (0.3 K) on different crystals in steady fields up to 18 T in Bristol, 33 T at the HFML in Nijmegen and in pulsed fields up to 56 T at the LNCMP, Toulouse.

Figs. 1a-b) show the field and temperature dependence of the torque signal and interlayer resistivity, respectively, performed with the magnetic field aligned close to the high symmetry easy  $c$  axis ( $\theta = 0$  when  $B \parallel c$ ). At low temperatures the torque signal varies as  $H^2$  in low fields suggesting that magnetization increases linearly with magnetic field. In higher fields we observed a series of kinks in torque (13.5 T, 20 T, 28.8 T and 38 T) which we attribute to magnetic phase transitions, similar anomalies have been seen at field-induced transitions in other uniaxial antiferromagnets [6]. The locations of the torque anomalies correlate closely with kinks seen in the interplane conduction, see Fig. 1b) (slightly shifted in field due to a difference in sample orientation), suggesting that the itinerant  $d$  electrons are highly sensitive to the changes in the magnetic order pattern.

A phase diagram constructed on the basis of torque, resistivity and specific heat measurements on several crystals is shown in Fig. 1e). The specific heat data shown in Fig. 1c confirm the transition between the paramagnetic (PM) and AFM phase at the Néel temperature  $T_N = 19.5$  K and a further strong anomaly at a lower temperatures (likely first-order), which co-

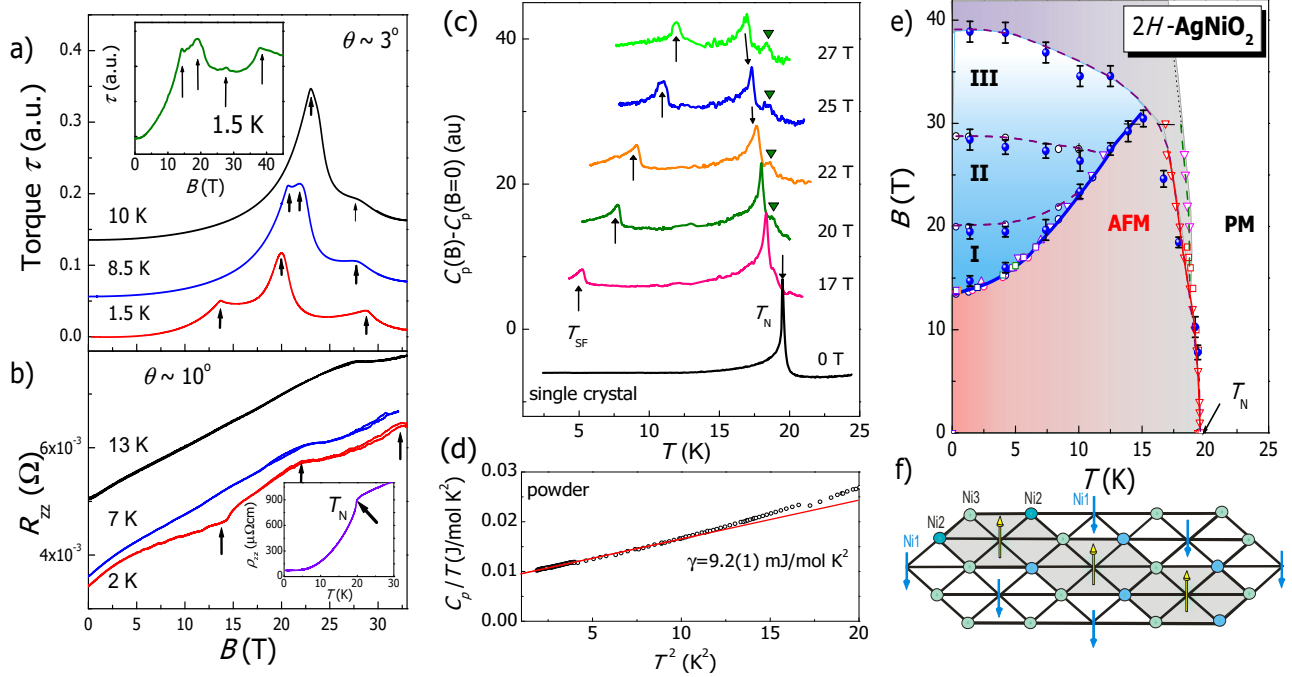


FIG. 1: (colour online) Field dependence of (a) the magnetic torque response, and (b) the interplane resistance at fixed temperatures when the magnetic field is close to the  $c$  axis ( $\theta \approx 3^\circ$  for torque measurements and  $\theta \approx 10^\circ$  for transport measurements)(sample B). The top inset show torque data in pulsed magnetic fields on a sample D and bottom inset shows the zero-field interplane resistance at low temperatures. Arrows indicate anomalies attributed to different magnetic transitions. (c) The relative variation of specific heat in different constant magnetic fields for sample C and (d) the low temperature extrapolation of  $C_p/T$  to in zero field for a powdered sample. The arrows indicate various transitions and the solid triangles corresponds to an additional transition in high fields. (e) Proposed phase diagram of  $2H\text{-AgNiO}_2$  from torque magnetometry (circles), specific heat (triangles), transport (square). The solid and dashed lines indicate boundaries between different magnetic phases: antiferromagnetic (AFM), high-field stabilized phases I, II, III, and paramagnetic (PM). A possible high field and high-temperature transition is also indicated (open triangles). The collinear magnetic structure (AFM phase) of Ni1 spins (arrows pointing up and down along  $c$ -axis) and honeycomb network for itinerant electrons is shown in (f).

incides with crossing the boundary separating the AFM and the higher field phase (I). In the limit of our experimental resolution (due to extremely small samples) we cannot detect clear signatures for the other two transitions (between phases I to II, and II to III), clearly observed both in the torque and transport measurements (Fig. 1a-b); this could be due to the fact that the specific-heat scans were performed mainly at constant temperature and transition boundaries are nearly flat and/or that these transitions are related to magnetic effects that do not involve a significant change in entropy.

The richness of the observed phase diagram is a manifestation of the complexity of magnetic interactions in the system. Besides the frustrated nature of triangular planar magnets,  $\text{AgNiO}_2$  is unique in the sense that it has several different magnetic interactions of disparate nature, but of the same scale. Indeed, since Ni1 ions are rather far apart, the superexchange between them is weak and cannot entirely dominate the physics of the system. On the other hand, the experimentally measured magnetic anisotropy gap is surprisingly large ( $\sim 1.7$  meV [7]) for a closed-shell ion, emphasizing the significant role of hybridization with Ni2,3 for magnetic interactions. Since Ni1 ions are embedded in a metal (Ni2 and Ni3),

they are subject to RKKY interaction, which, unlike superexchange, decays slowly with distance. For example, RKKY may provide non-negligible  $nnn$  Ni1 exchange, even to those ions that are too far apart for superexchange. Last but not least, the calculations show a small, but finite ( $0.1\text{-}0.2 \mu_B$ ) moment on the itinerant and inherently nonmagnetic Ni3 sites. The Hund rule coupling on these sites provides an additional incentive for Ni1s to order in such a way that the Ni3 moment be nonzero by symmetry (for instance, favoring the observed structure over the  $nn$ -only Heisenberg  $120^\circ$  structure). The scale of this interaction is set by the Hund's rule coupling energy on Ni3,  $Im^2/4$ , where the Stoner factor  $I \sim 0.6 - 0.8$  eV and  $m \sim 0.1 - 0.2 \mu_B$ , and appears to be a few meV. By a similar mechanism, the Hund's energy of induced moments generates ferromagnetism in  $\text{SrRuO}_3$  [8]. Note that a coupling between the conduction (Ni2,3) electrons and the local moments is evidenced by the significant drop in resistivity below  $T_N$ , as the result of suppression of electron scattering by low-energy spin fluctuations when a spin gap opens (see inset Fig. 1b). Moreover, the magnetoresistance shows changes in slope in the vicinity of the magnetic transitions (Fig. 1e), indicating significant scattering by the spin fluctuations close

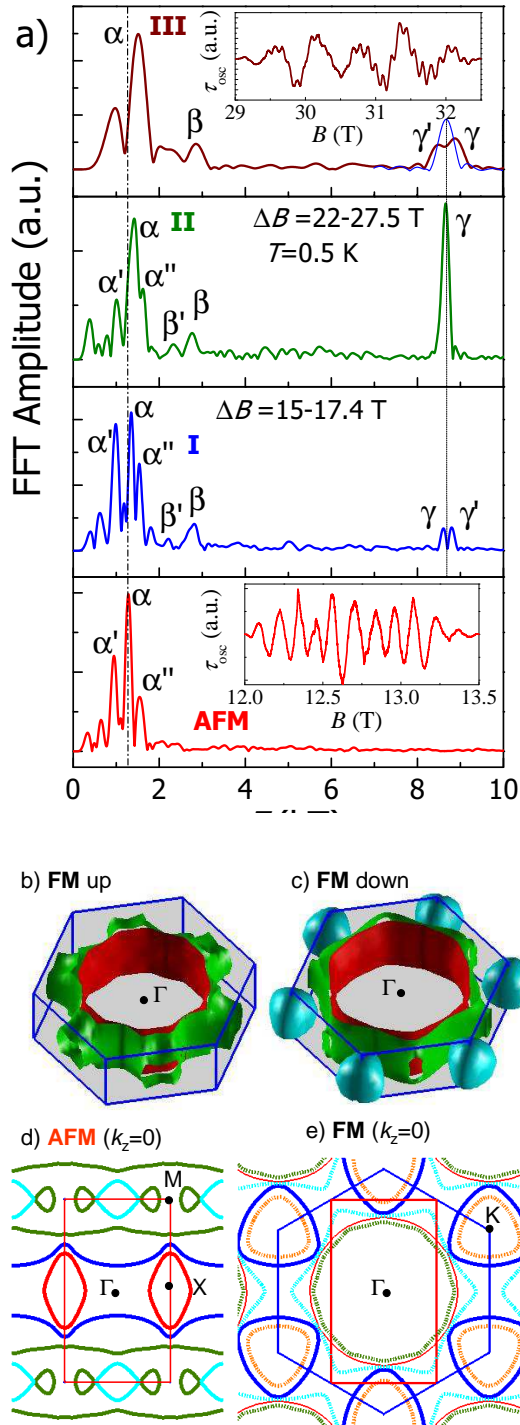


FIG. 2: (color online) (a) Fourier transformed spectra for different magnetic phases observed when the magnetic field is aligned close to the  $c$  axis ( $\theta \approx 3^\circ$  and  $T = 0.5(1)$  K). The raw dHvA data are shown as insets. Similar FFT windows ( $1/\Delta B$ ) were used up to 28 T (top panel shows a spectra of phase III compared with phase I for a similar field range (thin line)). The vertical lines are guides to the eye. (b) and (c) FS of the fully polarized configuration (see Ref.4) and slices of the (d) AFM and FM Fermi surface at the  $\Gamma$  point when the magnetic field is pointing along the  $c$  axis. The predicted orbits are shown (solid and dotted lines) inside the AFM (solid rectangle) and non-magnetic (hexagonal) Brillouin zone.

to these transitions. Finally, interplanar coupling (which also proceeds *via* the weakly-magnetic Ni3 ions [4]), while small, is not negligible either compared to other, in-plane interactions.

Even an oversimplified model of the localized Ni1 sublattice that includes only the on-site anisotropy, the  $nn$  exchange  $J$ , and a small  $nnn$  exchange  $J'$ , already demonstrates a surprising richness. Aside from the observed zero-field AFM collinear phase (Fig.1f) it allows for multiple phases in field, such as a modified version of the AFM phase, AFM', where the rows of up spins remain ferromagnetically aligned along the field  $\uparrow\uparrow\uparrow$  and the rows of down spins develop an additional weak transverse antiferromagnetic order as they tilt away from the easy axis  $\swarrow\searrow\swarrow$ . The AFM' configuration may be a candidate for phase I in Fig. 1e [9]. The mean-field critical field for the transition between AFM and AFM' is  $B_c = \Delta/g\mu_B$ ; note that the experimentally observed  $B_c = 13.5$  T (at low temperatures) agrees with this estimate, using  $\Delta = 1.7$  meV from neutron data [7] and assuming  $g = 2.17$ . One can show that at the mean-field level [9] the AFM' phase exists in a range of fields above  $B_c$  for  $J' > \Delta/12S$ , and is replaced by a honeycomb arrangement (spins aligned with the field on the honeycomb lattice with an anti-aligned spin on the central site). Other more complex phases manifest at higher fields, so that even in this highly simplified model there are multiple phases that can be stabilized by an external field, as seen in Fig. 1e. However, a more realistic model for AgNiO<sub>2</sub> would also need to account for the polarization of the itinerant electrons which brings in a Hund's rule energy term that can also distinguish between competitive phases. It is the itinerant Ni3 sites that provide the exchange link between successive layers so changes in the Ni3 polarization in field could also affect the 3D stacking of the magnetic order of the main Ni1 moments [4], and this might explain some of the higher-field transitions in Fig.1e.

If the itinerant  $d$  electrons are indeed important for the magnetic interaction and sensitive to the external field, one expects an interesting evolution of the Fermi surfaces with the field. We monitored this evolution using quantum oscillations in magnetic field. The total torque signal is dominated by the localized moment magnetism away from the easy axis and various magnetic phases have strong angular dependence in field [10], so here we concentrate on the behavior for fields close to the easy axis. De Haas-van Alphen oscillations are obtained by subtracting a fifth order polynomial from the total torque in different magnetic regions (see insets of Fig.2a). The Fourier transform allows us to identify the corresponding frequencies related to the extremal areas of the Fermi surface by the Onsager relation,  $F = (\hbar/2\pi e)A_k$ .

In the AFM phase the FFT spectra consist of closely packed frequencies below 2 kT with the most intense peak at  $\alpha \approx 1.3$  kT, see Fig. 2a). Above 13.5 T (phase I) additional split high frequencies appear,  $\gamma \approx 8.6$  kT, as well as  $\beta \approx 2.8$  kT (and a weak  $\beta'$ ). At much higher fields the spectra is composed of a similar number of frequencies, suggesting that the Fermi surface evolves rather smoothly above the first tran-

sition at 13.5 T. The  $\alpha$  pocket, occupies an area of  $\sim 8\%$  whereas  $\gamma$  occupies  $\sim 46\%$  of the non-magnetic Brillouin zone (hexagonal contour in Fig. 2d). In the AFM phase the Fermi surface is expected to be reconstructed by the collinear magnetic order ( $A_{AFM}=0.88 \times 10^{20} \text{ m}^{-2}$ ) and the  $\gamma$  pocket, if present, would occupy almost this entire magnetic zone area; however the  $\gamma$  pocket is not observed in the AFM phase suggesting that the Fermi surface is composed of small pockets that may result from reconstruction in the magnetic Brillouin zone [11].

Fig. 2d shows the calculated Fermi surface in the AFM phase (using the same computational methods as in Ref. 4). The FS is formed of a large number of small pockets with the largest predicted extremal areas corresponding to 1.7 kT (around the X point) which is in the range of values observed experimentally for the  $\alpha$  pocket. As the magnetic field is tilted away from the easy axis (towards the  $a$  axis) these low frequencies show sizable angular dependence in agreement with their complex quasi-2D and 3D origin [10].

In the high field phases, we consider the Fermi surface for a spin-polarized ferromagnetic (FM) ground state, where all magnetic spins are aligned (Figs.2b-d). This is also an approximation for an *unreconstructed* Fermi surface specific to  $\text{AgNiO}_2$  (note that because Ni1 sites are localized and strongly-magnetic means that a non-magnetic paramagnetic-like FS is not relevant here). This spin-polarized *large* Fermi surface is formed of quasi two-dimensional warped cylinders with and without neck orbits (centered around the  $\Gamma$  point) with large areas that can be assigned to  $\gamma$  pockets. Around the K point there is a quasi-three dimensional electronic pocket (of about 1 kT) similar to the  $\alpha$  pocket as well as orbits originating from the necks of the large cylinders that could explain the presence of  $\beta$  pockets (see Fig.2e). Thus, qualitatively, in high magnetic fields the observed FS pockets can be attributed to the large and small bands of the FM calculations. However, we would expect the new magnetic zone boundaries determined by the new magnetic order in phases I, II and III to open up new gaps on the Fermi surface. Observation of the high frequency  $\gamma$  in all these phases suggests that these gaps are small enough for the electrons to tunnel through, as the probability of tunnelling increases strongly in field, and the  $\gamma$  frequencies would correspond to magnetic breakdown orbits.

In a magnetic field and/or in the presence of the localized  $d$  electrons ( $\sim 1.5\mu_B$ ) the electronic bands will be shifted and/or split. As the system goes through different magnetic phases we observed that the  $\alpha$  pocket is slightly shifted towards higher values (see Fig.2a) whereas the splitting of the large  $\gamma$  pockets varies. If this split results from the spin-polarization of the quasi 2D bands (with similar shape centered at the  $\Gamma$  point in Fig.2e) by the local moments, then the direct exchange coupling estimated as  $\approx \hbar e \delta F / (2m^*)$  [12] varies from 1.62 meV in phase I to 3.21 meV in phase III, similar in magnitude to antiferromagnetic  $\text{NdB}_6$  where the localized  $f$  electrons are coupled to the conduction electrons [12]. This relatively small direct exchange splitting could explain the presence in the calculations of a small magnetic moment

$\sim 0.1 \mu_B$  on the itinerant Ni3 site [4].

In order to test whether electronic correlations are important we compare the measured  $\gamma$  of  $9.2(1) \text{ mJ/mol K}^2$  extracted from specific heat data (Fig.1d) with the calculated value of  $3.36(1) \text{ mJ/mol K}^2$  for the AFM phase. This gives a mass enhancement of  $\sim 2.6$ , close to that found in  $\text{Ag}_2\text{NiO}_2$  [13, 14] or  $\text{Sr}_3\text{Ru}_2\text{O}_7$  [15], suggestive of strong spin fluctuations. Using the Lifshitz-Kosevich formula [16] the effective mass for the  $\alpha$  pocket varies from  $\sim 2.3 m_e$  in the AFM phase to  $\sim 3.2 m_e$  in phase I. The effective mass of the  $\gamma$  pocket increases only slightly with the magnetic field from  $\sim 6.0 m_e$  (phase I) to  $\sim 6.6 m_e$  (phase III) reflecting the increase in magnetic susceptibility with magnetic field.

In conclusion, we report new rich physics induced by the magnetic field in  $2H\text{-AgNiO}_2$  as a result of the competition between strong easy-axis anisotropy, frustrated antiferromagnetic interactions and coupling between localized and itinerant electrons. The Fermi surface is reconstructed by the magnetic zones but in higher fields the gaps opened at the zone boundaries are small enough that the electrons can tunnel though. The corresponding effective masses are enhanced by a factor of  $\sim 3$  due to strong spin fluctuations. Similar physics could be relevant to other systems, such as the parent compounds of superconducting iron pnictides, where the rich physics observed can be determined by the interplay between local moment magnetism and itinerant electrons [17].

This work is supported by EPSRC (UK) and AIC is grateful to the Royal Society (UK) for financial support. Access to high magnetic field facilities has been supported by EuroMagNET II under EU contract.

- 
- [1] Y. Shimizu *et al.*, Phys. Rev. Lett. **91**, 107001 (2003).
  - [2] K. Takada *et al.*, Nature (London) **422**, 53 (2003).
  - [3] I. I. Mazin *et al.*, Phys. Rev. Lett. **98**, 176406 (2007)
  - [4] E. Wawrzynska *et al.*, Phys. Rev. Lett. **99**, 157204 (2007); *ibid* Phys. Rev. B **77**, 094439 (2008).
  - [5] T. Sorgel and M. Jansen, Z. Anorg. Allg. Chem. **631** 2970 (2005).
  - [6] T. Kawamoto *et al.*, Phys. Rev. B **77**, 224506 (2008)
  - [7] E.M. Wheeler *et al.* Phys. Rev. B **79**, 104421 (2009).
  - [8] I. I. Mazin and D. J. Singh, Phys. Rev. 1997, B56, 2556
  - [9] L. Seabra *et al.*, J. Phys.: Conf. Series, **145**, 012075 (2009). L. Seabra, private communication.
  - [10] A.I. Coldea *et al.*, in preparation (2009).
  - [11] The  $\gamma$  frequencies ( $\sim 6m_e$ ) are damped out exponentially by the impurity scattering so they may not be observed in low magnetic fields but studies up 45 T in the AFM phase fail to reveal the  $\gamma$  frequency [10].
  - [12] R. G. Goodrich and N. Harrison and Z. Fisk, Phys. Rev. Lett., **97** 146404 (2006).
  - [13] M. D. Johannes *et al.*, Phys. Rev. B **75**, 180404, (2007).
  - [14] H. Yoshida *et al.*, Phys. Rev. B **73**, 020408 (2006)
  - [15] R. A. Borzi *et al.* Phys. Rev. Lett., **92** 216403 (2004).
  - [16] D. Shoenberg, *Magnetic Oscillations in Metals* (Cambridge Univ. Press, Cambridge, 1984).
  - [17] J. Zhao *et al.*, Nature Physics **5**, 555 (2009)